Floating substructure flexibility of large-volume 10MW offshore wind turbine platforms in dynamic calculations

Borg, Michael; Hansen, Anders Melchior; Bredmose, Henrik

Published in:
Journal of Physics: Conference Series (Online)

Link to article, DOI:
10.1088/1742-6596/753/8/082024

Publication date:
2016

Document Version
Publisher's PDF, also known as Version of record

Floating substructure flexibility of large-volume 10MW offshore wind turbine platforms in dynamic calculations

Michael Borg, Anders Melchior Hansen, Henrik Bredmose
DTU Wind Energy, Technical University of Denmark, Kgs. Lyngby, Denmark
E-mail: borg@dtu.dk

Abstract. Designing floating substructures for the next generation of 10MW and larger wind turbines has introduced new challenges in capturing relevant physical effects in dynamic simulation tools. In achieving technically and economically optimal floating substructures, structural flexibility may increase to the extent that it becomes relevant to include in addition to the standard rigid body substructure modes which are typically described through linear radiation-diffraction theory. This paper describes a method for the inclusion of substructural flexibility in aero-hydro-servo-elastic dynamic simulations for large-volume substructures, including wave-structure interactions, to form the basis of deriving sectional loads and stresses within the substructure. The method is applied to a case study to illustrate the implementation and relevance. It is found that the flexible mode is significantly excited in an extreme event, indicating an increase in predicted substructure internal loads.

1. Introduction

In pursuing reductions in the levelized cost of wind energy, the offshore wind industry is moving towards larger wind turbine units in the range of 10MW to exploit better wind resources found offshore. In deeper waters, floating foundations typically become the more economically feasible option over fixed foundations to support the wind turbine unit. Technically and economically optimal floating foundations for such large wind turbines may result in increased structural flexibility of the floating substructure.

To date, preliminary design and optimization studies that involve fully coupled aero-hydro-servo-elastic simulations for up to 5MW machines have considered the substructure to be rigid. This has been a suitable assumption given the dimensions of such platforms, coupled with design practices adopted from the offshore oil and gas industry. Furthermore this approach has been practical, with the representation of the floating substructure as a single point six degree-of-freedom (DOF) body within dynamic simulations. The structural design of the substructure is then decoupled from the dynamic simulations and equivalent static load cases are considered. This is seen in previous work for the WindFloat concept [1], Dutch tri-floater [2] and a spar [3].

With the increased external dimensions of floating substructures for 10MW wind turbines, the present study goes a step further and investigates the inclusion of substructure flexibility in aero-hydro-servo-elastic simulations for preliminary design and optimization of large-volume floating substructures. The goal is to migrate from the current decoupled process to coupled aero-hydro-

servo-elastic simulations that includes flexible modes and thus integrates the structural design and analysis of the floating substructure.

The aim of the paper is twofold: First we establish the straightforward use of a radiation-diffraction solver to achieve hydrodynamic generalized forcing and coefficients of flexible DOFs, and the subsequent inclusion within a coupled simulation tool. Next the implementation is used to evaluate the influence of this motion on the dynamic response of a floating wind turbine.

The HAWC2 aeroelastic simulation tool, coupled with the wave-structure interaction analysis tool WAMIT, are used for carrying out simulations and analyses. HAWC2 has been previously used for simulating the dynamic response of a number of floating wind turbine concepts [8], and has been compared against other floating wind turbine simulation tools [9] and scale model measurements [10]. The HAWC2-WAMIT model complex is described in [8].

The paper is organised as follows: first a brief overview of the relevant theoretical background is presented, followed by a description of the numerical implementation within the coupled simulation tool. A case study and analysis are then presented, concluding with a discussion of the results.

2. Theoretical Background

Different hydrodynamic numerical models are applicable for floating wind turbines that depend on flow regimes and the relative size of the structure with respect to wavelength [4]. The Morison equation [5] has been widely used for slender structures, whilst linear potential flow theory solved through boundary element methods has been used to derive the radiation and diffraction forces, and motion responses of large-volume structures. In the case of the latter method, the potential flow solution is typically linearized at an equilibrium position for the structure and a harmonic solution to the velocity potential is assumed. The velocity potential is decomposed into a number of components that represent the incident (Φ_i), diffracted (Φ_d), and radiated (Φ_r) wave fields, Eqn. (1).

$$\Phi(x, y, z, t) = \Phi_i + \Phi_d + \Phi_r \tag{1}$$

The incident wave field potential is defined through linear gravity wave theory; the diffraction wave field potential represents the wave scattering due to the structure, assumed fixed at the equilibrium position; and the radiated wave field potential represents waves generated by motion in each body DOF. The conventional rigid-body DOFs, that is, surge, sway, heave, roll, pitch and yaw, are denoted by $j = 1, 2, ..., 6$. This notation is similarly followed for additional N body deformation DOFs. For all $(6 + N)$ modes a separate shape function, $\mathbf{S}_{ij} = [u_{ij} \quad v_{ij} \quad w_{ij}]$, is defined that relates the displacement of the i'th panel on the body surface to a displacement in the j'th mode, ξ_j. Given the unit normal vector $\mathbf{n}_i$ of the i'th panel on the submerged structure surface S_b, the normal component of $\mathbf{S}_{ij}$ on S_b can be determined:

$$n_{ij} = \mathbf{S}_{ij} \cdot \mathbf{n_i} = u_{ij} n_x + v_{ij} n_y + w_{ij} n_z \tag{2}$$

The radiation wave field potential Φ_r is composed of a linear superposition of contributions from motion in all $(6 + N)$ modes, Eqn. (3).

$$\Phi_r = \sum_{j=1}^{6+N} \xi_j \phi_j \tag{3}$$

Here ϕ_j represents the unit-amplitude radiation potential in the j'th mode. On the undisturbed position of the body boundary, the radiation and diffraction potentials are subject to:

$$\frac{\partial \phi_j}{\partial n} = i\omega n_j \tag{4}$$

$$\frac{\partial(\phi_d + \phi_i)}{\partial n} = 0 \tag{5}$$

By application of linearized boundary conditions at the seabed and free surface, as well as a far-field boundary condition, the relevant hydrodynamic coefficients can be calculated. For further detail, the reader is referred to [6]. Wave-structure interaction analysis software programs such as WAMIT [7] solve the above in the frequency domain and the hydrodynamic coefficients relevant to evaluating the dynamic response of a flexible structure include the added mass, damping and hydrostatic stiffness matrices, as well as the velocity potential and generalised exciting forces for all $(6 + N)$ modes.

3. Implementation

In HAWC2, a large-volume floating body is represented through the Cummins equation [11]. An interface between HAWC2 and WAMIT has been previously set up to provide the necessary information for the construction of the matrix terms within the Cummins equation. In this work, this interface has been extended to accommodate the additional flexible degrees of freedom prescribed in WAMIT such that Eqn. (6) governs $(6 + N)$ states.

$$(\mathbf{M} + \bar{\mathbf{A}}_\infty)\ddot{\mathbf{x}}(t) + \int_0^t \bar{\mathbf{K}}\,(t-\tau)\,\dot{\mathbf{x}}(\tau)d\tau + \bar{\mathbf{C}}\mathbf{x}(t) = \mathbf{F}(\mathbf{x}, \dot{\mathbf{x}}, t) \tag{6}$$

Here, $\mathbf{M}$, $\bar{\mathbf{A}}_\infty$, $\bar{\mathbf{C}}$ are the generalized structural mass, infinite-frequency added mass, and stiffness matrices, respectively, $\bar{\mathbf{K}}$ is the radiation force retardation function matrix, and $\mathbf{F}$ is the generalized force vector. In the HAWC2 multibody formulation, the relation between the wind turbine model, in this case the tower base, and the floating substructure is governed by displacement constraints for the six DOF rigid body motion at the connection point. This is then represented as a constraint force in the first six states in Eqn. (6) and subsequently influencing the additional flexible modes through the off-diagonal elements within system matrices. In addition to the extension of the original interface for time-domain coupled simulations, additional preprocessing steps were required to derive the necessary structural input to WAMIT. Figure 1 outlines this process. The preprocessing procedure is described in more detail below.

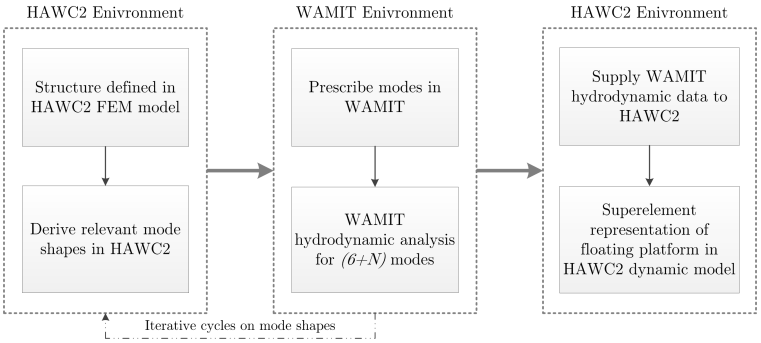

Figure 1. Interactions between HAWC2 and WAMIT

Step I. First we construct a finite element (FE) model of the whole floating wind turbine system in HAWC2. For the definition of hydrodynamic added mass on the substructure, we apply the theoretical value from the Morison equation based on the local diameter of the submerged section. The structural eigenvalue problem is then solved to establish the system eigenvalues and eigenmodes.

Step II. Next we use knowledge of the relation between the WAMIT panels and the FE model to derive the relevant shape functions $\mathbf{S}_{ij}$ described earlier. In this implementation, a

Timoshenko beam-type FE model is utilised in HAWC2, that may consist of a number of bodies, and as such a fixed relation between the body centerline and an arbitrary point on the cross section exterior is assumed. A right-handed Cartesian coordinate system is used and the generalized position along the length of the body is used as a reference, which allows for both straight and curved bodies in three dimensions to be considered. With the displaced position of the body centerline, $\mathbf{u}_{ij}$, and the position of the i'th panel centroid relative to the centerline, $\mathbf{x}_i$, the displacement of the i'th panel centroid due to the j'th mode, $\mathbf{r}_{ij}$, can be calculated from:

$$\mathbf{r}_{ij} = \mathbf{u}_{ij} + \mathbf{R}_{3ij}\mathbf{R}_{2ij}\mathbf{R}_{1ij}\mathbf{x}_i \tag{7}$$

Here $\mathbf{R}_{3ij}$, $\mathbf{R}_{2ij}$ and $\mathbf{R}_{1ij}$ are j'th mode Euler angle transformation matrices about the z, y and x axes, respectively. Figure 2 illustrates this step for a section of a cylindrical panel model.

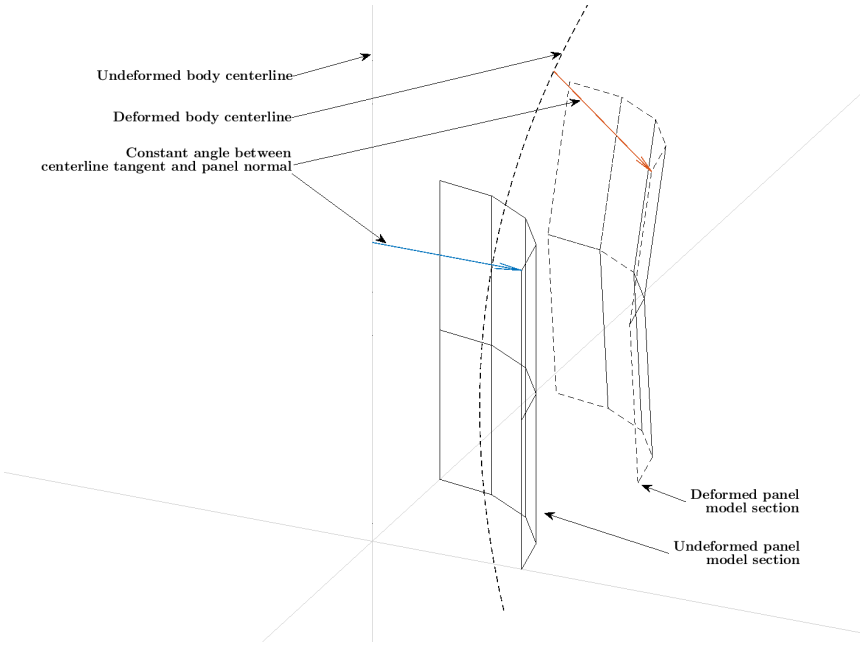

Figure 2. Illustration of displaced panel model section

Step III. We then define the panels centroid displacements as a function of mode in WAMIT through the `NEWMODES` subroutine [7] and the necessary wave-structure interaction analysis is carried out. The added mass distribution in the HAWC2 FE model is then updated based on this analysis. This is done by extracting the added mass contribution from the velocity potential on each panel, and mapping this distribution to the FE model. The mapping function largely depends on the detail of the FE model, and in the present implementation we derive an equivalent added mass per unit length for each beam element. The infinite-frequency added mass rather than the added mass at the mode eigenvalue is considered here for practical reasons. Whilst it would be ideal to make use of the added mass at the mode eigenvalue, this can be impractical for some mode shapes that have very high eigenvalues, and thus would radiate waves of very short wavelengths. This would then require a very fine mesh resolution within the potential flow solver, which may lead to numerical inaccuracies and excessive computational resources. Hence the asymptotic infinite-frequency value is used to enable a more robust iterative process to estimate the wet eigenmodes. Often this is a good approximation to wet eigenmode added mass as can later be seen in Figure 5.

Step IV. We re-evaluate the eigenvalue problem to establish improved mode shapes and repeat **Steps II** and **III** until convergence is achieved.

The iterative procedure detailed above is necessary as the added mass distribution is not known a priori, and depends on the flexible mode shape. While the natural modes are calculated in the FE model, the added mass is computed in WAMIT. Lastly, as we are interested in capturing the correct mode shapes of the structure, the convergence criterion in **Step IV** is based on the evaluated mode shapes. Here we used linear regression to evaluate the convergence of each mode shape, with the criterion of 0.999 R-squared value must be achieved between successive iterations.

4. Case Study

The scope of the case study is to compare the loads of the a wind turbine considering a rigid substructure, and a flexible substructure.

4.1. Substructure design

A hypothetical floating spar was sized to support the DTU 10MW Reference Wind Turbine [12]. The design focused on providing sufficient platform pitch stability. Furthermore, a relatively low first bending frequency was established such that hydrodynamic forcing of this mode is possible. This is by no means the optimal design methodology one should consider, but for the case of this work it was useful to illustrate the behaviour of a simple flexible mode. A simple linear mooring model was applied in surge, sway and yaw at the tower-substructure interface to restrain the substructure from excessive excursions on the sea surface. Stiffness values were chosen such that the surge and sway natural periods were 100 seconds and the yaw natural period was 8.5 seconds. Figure 3 and Table 1 provide the main dimensions and characteristics of the design. In this case study one additional flexible mode was considered and corresponds to the first in-plane bending mode of the floating wind turbine system, depicted in Figure 4.

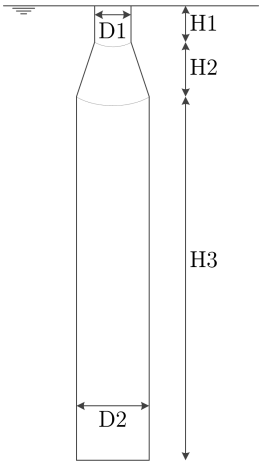

Figure 3. Spar geometry

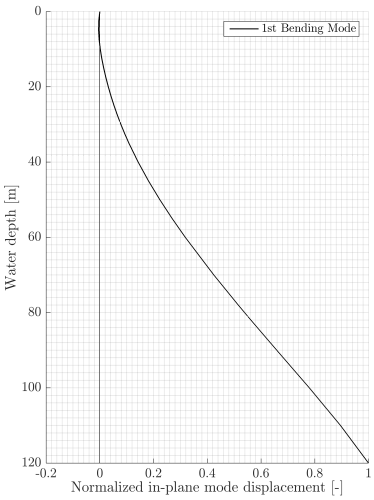

Figure 4. Normalized spar in-plane bending mode

4.2. Load cases & environmental conditions

A number of different environmental conditions were simulated in this study. These consisted of white-noise waves with no wind, and a parked condition in a focused wave without wind. In all

cases the waves were unidirectional. Table 2 presents the relevant environment and simulation parameters, with load case 2 obtained from [13].

Parameter	Value	Parameter	Value
Substructure		Wind turbine [12]	
Draft [m]	120.0	RNA mass [t]	676.7
Displacement [m^3]	1.59×10^4	Hub height [m]	119.0
Material	Steel	Tower mass [t]	628.4
Material density* [kg/m^3]	8500	Material	Steel
H1 [m]	15.0	Top diameter	5.5
H2 [m]	20.0	Base diameter [m]	8.3
H3 [m]	85.0		
D1 [m]	8.3		
D2 [m]	14.0		
Lin. mooring stiffness [N/m]	1.22×10^5		
Rot. mooring stiffness [Nm/rad]	1.62×10^9		

*incld. secondary structures

Table 1. Floating wind turbine dimensions

4.3. Transfer functions

Figure 5 presents the normalized added mass and damping computed by WAMIT for surge, heave, pitch, bending mode and DOF couplings. Figure 6 presents the normalized wave excitation force transfer functions for the in-line DOFs computed by WAMIT, namely, surge, heave, pitch and the bending mode. Figure 7 presents the motion response amplitude operators (RAOs) for surge, heave and pitch substructure motion with and without the flexible mode considered within the dynamic simulation for the full floating wind turbine structure.

One can note that the added mass and damping computed for the flexible mode largely follows the trend of the values computed for pitch motion. This is to be expected, as the largest flexible mode deflections occur at the end of the substructure, cf. Figure 4, which is furthest away from the reference system origin located at the point of flotation at the mean water level.

From the RAOs presented in Figure 7, it can be seen that the inclusion of the flexible mode increases the response of surge, heave and pitch, most significantly at their respective natural frequencies. The flexible mode RAO is dominated by response at the surge and pitch natural frequencies, as there are strong couplings present with these rigid-body DOFs. The smaller peak seen at 1 Hz relates to the flexible mode natural frequency.

No.	Type	H [m]	Duration [s]
1	White noise	2.0	10800.0
2	Focused Wave	18.84	500.0

Table 2. Simulation conditions

4.4. Transient response

Here we investigate the response of the floating wind turbine to a transient, extreme event represented by a focused wave. Figure 8 presents the dynamic response of substructure surge,

pitch, flexible mode deformation, wind turbine nacelle acceleration and tower base bending moment in the time and frequency domain. Results for both rigid and flexible substructure HAWC2 models are included. The global motion response in surge and pitch do not appear to be significantly changed by the inclusion of the first substructure bending mode, with the responses dominated by an initial forced oscillation followed by a free decay at the surge- and pitch-dominated eigenvalues. In the case of the flexible mode, ξ_7, only a forced response is observed in the range of significant wave energy frequency content. Some energy content is also present at the surge, pitch and flexible mode eigenvalues, however at one to two orders of magnitude lower than the forced wave response. This follows from the observations made in the RAOs of these DOFs.

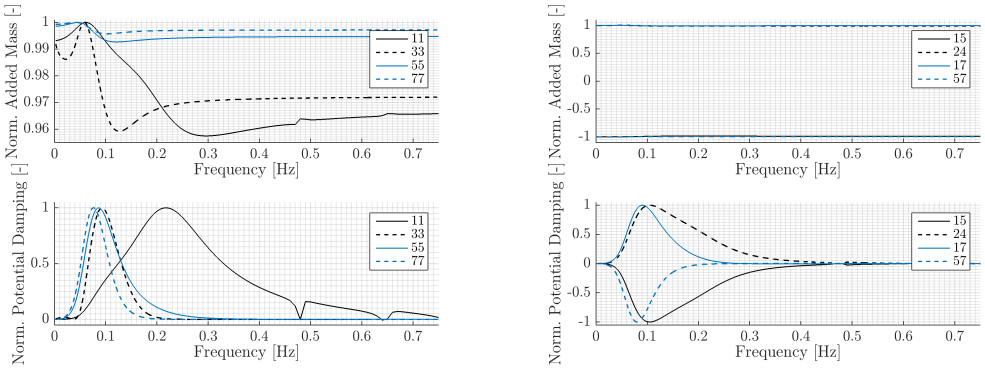

Figure 5. Hydrodynamic coefficients computed by WAMIT

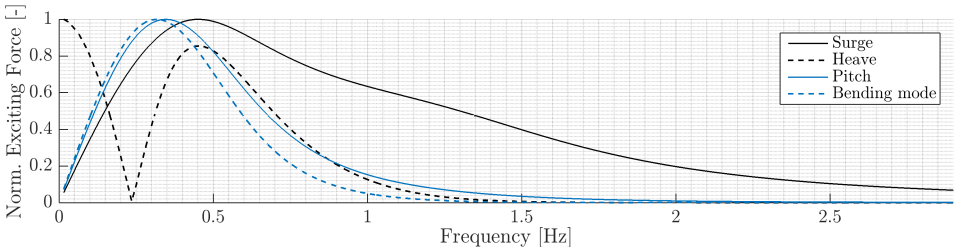

Figure 6. Wave excitation force transfer functions computed by WAMIT for zero degree wave heading

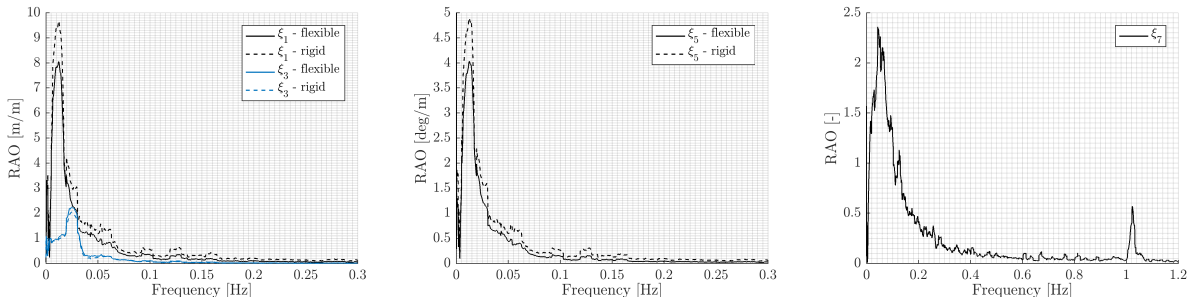

Figure 7. Comparison of motion response amplitude operators from HAWC2 waves-only white-noise simulation

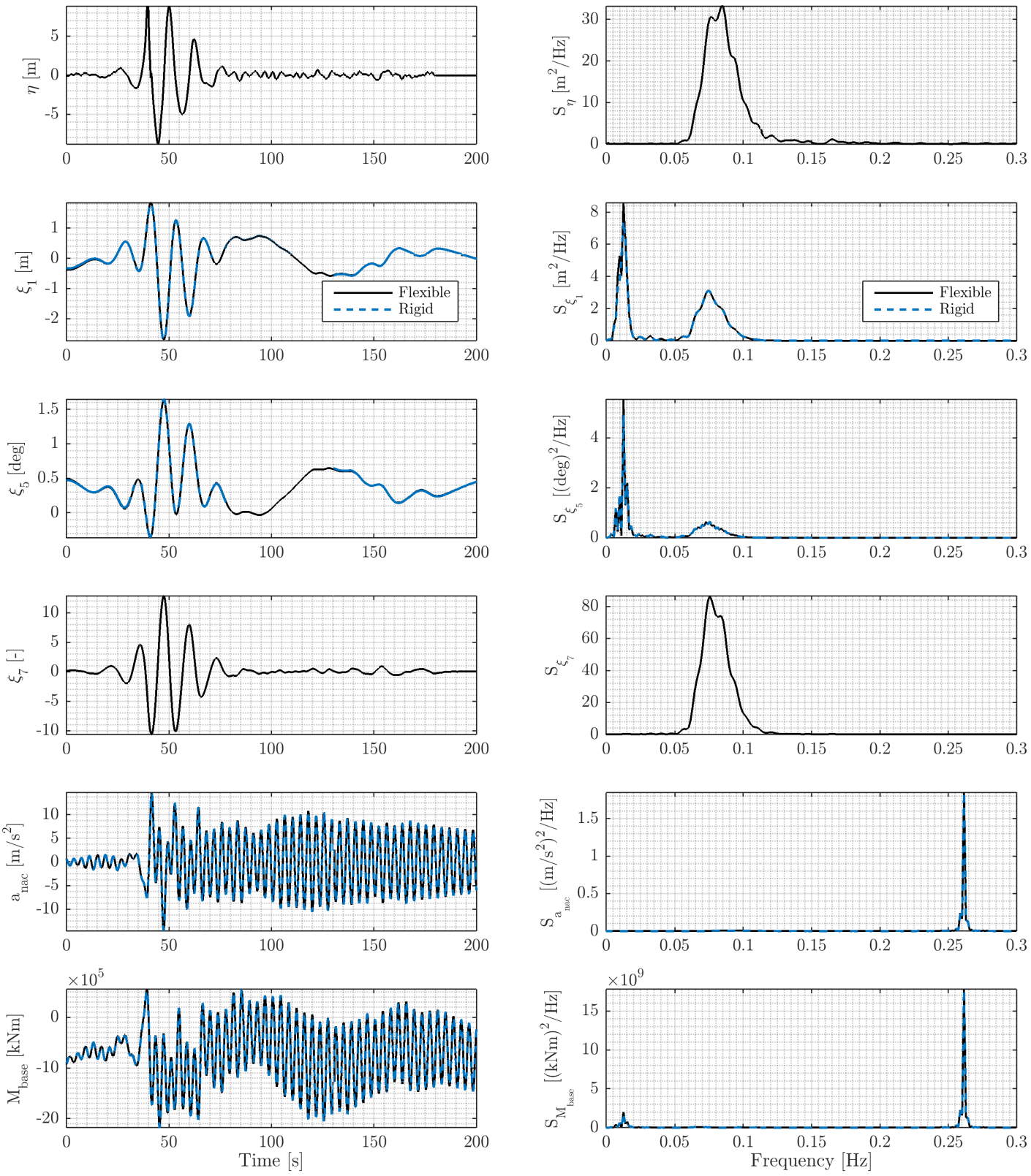

Figure 8. Flexible and rigid substructure models responses to a focused wave event

On the other hand, the wind turbine response is dominated by the first tower bending frequency - an implusive excitation is experienced by the wind turbine upon impact of the focused wave. This is visible both in the nacelle acceleration and tower base moment. Some response in the tower base bending moment at the substructure eigenvalues is observed, as the dominant peak responses in surge and pitch are also at these frequencies. Due to the tower flexibility this secondary response frequency is not significant for nacelle acceleration, which is dominated by the tower bending frequency.

5. Future work

The present work represents the first step in coupling substructure structural design with aero-hydro-servo-elastic dynamic simulations typically carried out in the preliminary stages of the design cycle of a floating wind turbine. With the HAWC2 implementation established here, future work will focus on the calculation of internal loads and stresses in the substructure on the basis of dynamic simulations.

6. Conclusions

This work illustrated the straightforward use of a radiation-diffraction solver to incorporate flexibility of large-volume floating substructures within floating wind turbine dynamic calculations. The implementation within the HAWC2 aeroelastic tool coupled with WAMIT and the procedure for establishing a dynamic flexible substructure model were detailed.

A conceptual spar-type floating substructure with the DTU 10MWW reference wind turbine was considered to investigate the inclusion of flexible substructure modes within dynamic calculations. In this case study it was seen that the first substructure bending mode was coupled with pitch motion, and whilst motion in this flexible mode did not have a significant effect on the global substructure and wind turbine responses, substantial forcing and excitation of this mode indicates that sectional loading within the substructure can be dependent on such motion.

It is important to note that the above observations are specific to the spar used in this work, and as such other substructures may have different influences on the wind turbine response. This work has shown that the inclusion of flexible modes within dynamic calculations of large-volume substructures for floating wind turbines provides additional information on the dynamic behaviour of the substructure and can assist to derive more accurate sectional loads for structural design. The natural next step following this work will establish a methodology for the calculation of sectional loads and stresses in the substructure based on dynamic simulations and external pressure loads within a detailed FE model.

Acknowledgments

This project has received funding from the European Unions Horizon 2020 research and innovation programme under grant agreement No 640741 (LIFES50+).

References

[1] Roddier D, Cermelli C, Aubault A, Weinstein A (2010). WindFloat: a floating foundation for offshore wind turbines. *Journal of Renewable and Sustainable Energy*, **2**, 033104.

[2] Lefebvre S, Collu M (2012). Preliminary design of a floating support structure for a 5MW offshore wind turbine. *Ocean Engineering*, **40**, p.15-26.

[3] Hu Z, Liu Y, Wang J (2016). An integrated structural strength analysis method for spar type floating wind turbine. *China Ocean Eng.*, **30**, *2*, p.217-230.

[4] Borg M, Bredmose H (2015). Overview of the numerical models used in the consortium and their qualification. *LIFES50+ Deliverable 4.4, DTU Wind Energy Report-E-0097*, Technical University of Denmark, Kgs. Lyngby, Denmark.

[5] Morison JR, O'Brien MB, Johnson JW, Schaaf SA (1950). The force exerted by surface waves on piles. *Pet Trans*, **189**, p.149-154.

[6] Newman JN (1994). Wave effects on deformable bodies. *Applied Ocean Research*, **16**, p.47-59.
[7] http://wamit.com/
[8] Larsen TJ, Yde A, Verelst D, Pedersen MM, Hansen AM, Hansen HF (2014). Benchmark comparison of load and dynamics of a floating 5MW semisub windturbine, using three different hydrodynamic approaches. *DTU Wind Energy Report-I-0239*, Technical University of Denmark, Roskilde, Denmark.
[9] Robertson A, Jonkman J, Vorpahl F, et al. (2014). Offshore code comparison collaboration continuation within IEA Wind Task 30: phase II results regarding a floating semisubmerisble wind system. *33rd International Conference on Ocean, Offshore and Arctic Engineering*, San Francisco, California.
[10] Kocaturk AS (2015). Numerical study of the DTU 10MW floating wind turbine on a TLP platform. *DTU Wind Energy Master Thesis M-0093*, Technical University of Denmark, Roskilde, Denmark.
[11] Cummins WE (1962). The impulse response function and ship motions. *Symposium on Ship Theory*, Institut fur Schiffbau, Universitat Hamburg.
[12] Bak C, Zahle F, Bitsche R, Kim T, Yde A, Henriksen LC, Natarajan A, Hansen MH (2013). Description of the DTU 10MW reference wind turbine. *DTU Wind Energy Report-I-0092*, Technical University of Denmark, Roskilde, Denmark.
[13] Pegalajar-Jurado A, Bredmose H, Borg M (2016) Multi-level hydrodynamic modelling of a scaled 10MW TLP wind turbine. *Energy Procedia (in press)*.
[14] Bredmose H, Slabiak P, Sahlberg-Nielsen L, Schlütter F (2013). Dynamic excitation of monopiles by steep and breaking waves. Experimental and numerical study. *Proceedings of ASME 2013 32nd International Conference on Ocean, Offshore and Arctic Engineering*, Nantes, France.